Bestrophin-2 is a candidate calcium-activated chloride channel involved in olfactory transduction

Simone Pifferi*†, Giovanni Pascarella†‡, Anna Boccaccio*, Andrea Mazzatenta*, Stefano Gustincich‡, Anna Menini*§, and Silvia Zucchelli‡

*Sector of Neurobiology, International School for Advanced Studies (SISSA), Via Beirut 2-4, 34014 Trieste, Italy; and ‡Giovanni Armenise–Harvard Foundation Laboratory, Sector of Neurobiology, International School for Advanced Studies (SISSA), AREA Science Park, S.S. 14, Km 163.5, Basovizza, 34012 Trieste, Italy

Edited by Joseph A. Beavo, University of Washington School of Medicine, Seattle, WA, and approved July 5, 2006 (received for review June 2, 2006)

Ca-activated Cl channels are an important component of olfactory transduction. Odor binding to olfactory receptors in the cilia of olfactory sensory neurons (OSNs) leads to an increase of intraciliary Ca concentration by Ca entry through cyclic nucleotide-gated (CNG) channels. Ca activates a Cl channel that leads to an efflux of Cl from the cilia, contributing to the amplification of the OSN depolarization. The molecular identity of this Cl channel remains elusive. Recent evidence has indicated that bestrophins are able to form Ca-activated Cl channels in heterologous systems. Here we have analyzed the expression of bestrophins in the mouse olfactory epithelium and demonstrated that only mouse bestrophin-2 (mBest2) was expressed. Single-cell RT-PCR showed that mBest2 was expressed in OSNs but not in supporting cells. Immunohistochemistry revealed that mBest2 was expressed on the cilia of OSNs, the site of olfactory transduction, and colocalized with the main CNGA2 channel subunit. Electrophysiological properties of Ca-activated Cl currents from native channels in dendritic knob/cilia of mouse OSNs were compared with those induced by the expression of mBest2 in HEK-293 cells. We found the same anion permeability sequence, small estimated single-channel conductances, a Ca sensitivity difference of one order of magnitude, and the same side-specific blockage of the two Cl channel blockers commonly used to inhibit the odorant-induced Ca-activated Cl current in OSNs, niflumic acid, and 4-acetamido-4′-isothiocyanato-stilben-2,2′-disulfonate (SITS). Therefore, our data suggest that mBest2 is a good candidate for being a molecular component of the olfactory Ca-activated Cl channel.

ion channel | olfaction | olfactory sensory neurons | patch–clamp | sensory coding

The initial steps of olfaction occur in olfactory sensory neurons (OSNs), located in the olfactory epithelium (OE) of the nasal cavity. OSNs are responsible for the detection of odorant molecules present in the environment and the generation of the neural signal that is transmitted to the brain (for reviews, see refs. 1–3). OSNs are bipolar neurons with a single dendrite that terminates with a knob, from which protrude several tiny cilia, where the transduction of the olfactory signal takes place. Odorant molecules bind to olfactory receptor proteins, and this interaction triggers an increase in the ciliary concentration of cAMP through the activation of receptor-coupled G protein and adenylate cyclase. Cyclic nucleotide-gated (CNG) channels located in the ciliary membrane are directly activated by cAMP, causing a depolarizing influx of Na and Ca ions. It is well known that Ca-activated Cl channels are present in the ciliary membrane (4, 5), and that the increase in Ca concentration inside the cilia activates a Cl current (4–7). OSNs maintain an unusually high internal concentration of Cl that is in the same range of the Cl concentration present in the mucus at the external side of the cilia (8–11). In physiological conditions, the opening of Ca-activated Cl channels in the ciliary membrane causes an efflux of Cl ions from the cilia, corresponding to an inward current that further contributes to the depolarization of OSNs (4–7). During olfactory transduction, the secondary Ca-activated Cl current plays the important role of a high-gain and low-noise amplifier of the primary CNG current (ref. 12; for reviews, see refs. 13–15), contributing between 50% and 85% of the total odorant-induced current (6, 7, 11). Nevertheless, the molecular players of Cl homeostasis in OSNs are still elusive. Only recently, it has been shown that NKCC1, a Na-K-2Cl cotransporter, is implicated in the maintenance of a high Cl concentration inside OSNs (16, 17), although another study indicates the possibility that NKCC1 is not the only component involved in this process (18).

The molecular identity of the Ca-activated Cl channel involved in olfactory transduction is still obscure. Bestrophins from several species produce Ca-activated Cl currents when expressed heterologously (refs. 19–26; for review, see ref. 27). In the mouse, this gene family comprises three genes (mBest1, -2, and -4) and a pseudogene (mBest3; ref. 28). In humans, several different mutations in bestrophin-1 cause bestrophin vitelliform macular dystrophy (refs. 29 and 30; for review, see refs. 20 and 31).

The biophysical properties of mBest2 have been recently investigated with the patch–clamp technique, showing that mBest2 by itself forms Ca-activated Cl channels in heterologous systems and is a structural component of the ion-conducting pore. Bestrophin-2 can thus be considered a bona fide Cl channel (21, 22, 26, 32).

We demonstrate here that mBest2 mRNA is expressed in OSNs, and that the mBest2 protein is located on the cilia, where olfactory transduction occurs. On the cilia, mBest2 colocalizes with CNGA2, the main subunit of the olfactory CNG channel (for review, see ref. 33). We measured, with the patch–clamp technique, the functional properties of the current induced by heterologous expression of mBest2 and those of the native Ca-activated Cl current from dendritic knob/cilia of mouse OSNs. The colocalization of mBest2 with CNGA2 on the cilia and the similarities of some functional properties of mBest2 currents with those of the native olfactory Ca-activated Cl channels indicate mBest2 is a good candidate for being a molecular component of the olfactory Ca-activated Cl channel.

Results

Bestrophin-2 Is Expressed in OSNs. Bestrophins have been proposed to constitute a new family of Ca-activated Cl channels (for review, see ref. 27). In the mouse, the bestrophin family is composed of three coding genes (mBest1, -2, and -4) and one pseudogene (mBest3; see ref. 28). We screened the expression of mBest1, -2, and -4 in the OE by RT-PCR (Fig. 1*a*). In this tissue, we detected the expression of mRNA of mBest2 but not of

Conflict of interest statement: No conflicts declared.

This paper was submitted directly (Track II) to the PNAS office.

Abbreviations: OSN, olfactory sensory neuron; OE, olfactory epithelium; CNG, cyclic nucleotide-gated; mBest2, mouse bestrophin-2; NFA, niflumic acid; SITS, 4-acetamido-4′-isothiocyanato-stilben-2,2′-disulfonate; MeS, methanesulfonate.

†S.P. and G.P. contributed equally to this work.

§To whom correspondence should be addressed. E-mail: menini@sissa.it.

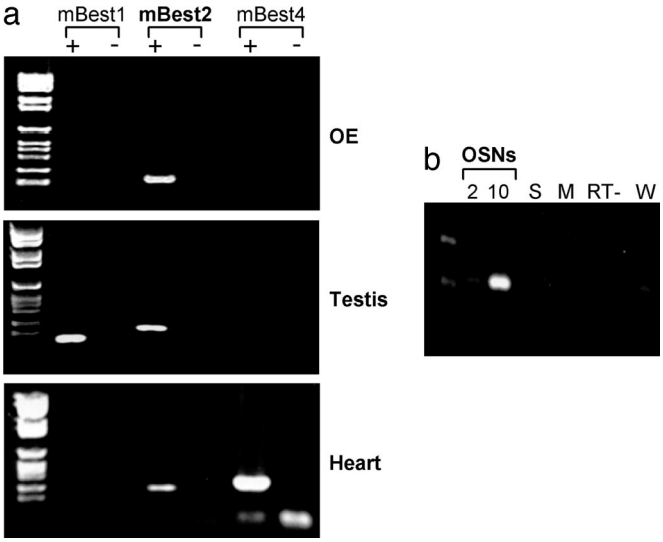

Fig. 1. mBest2 is expressed in mouse OSNs. (*a*) Primers specific for mBest1, -2, and -4 were used to amplify cDNA obtained from RNA of OE, testis, and heart. (*b*) Primers specific for mBest2 were used to amplify cDNA made from RNA of 2 OSNs, 10 OSNs, and 10 supporting cells (S). Other negative controls are resuspension media for OSNs (M), retrotranscriptase free sample (RT−) and water-only sample (W).

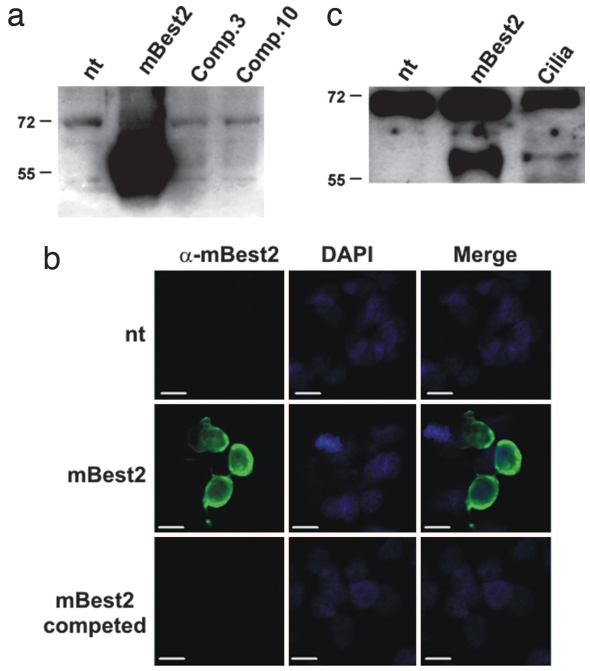

Fig. 2. Expression of mBest2 in transfected HEK-293 cells, anti-mBest2 antibody specificity, and expression of mBest2 in olfactory cilia preparation. HEK-293 cells were transiently transfected with mBest2, and the specificity of α-mBest2 antibody was demonstrated by competing the specific mBest2 signal with incubation of 3 or 10 μg of purified GST-mBest2 in Western blot (*a*) or with 30 μg of purified mBest2 in immunofluorescence (*b*). (Scale bar, 10 μm.) (*c*) Expression of mBest2 in olfactory cilia was detected by Western blot analysis using a cilia-enriched preparation.

mBest1 and -4. As controls, we identified mRNAs of mBest1 and -2 in the testis and of mBest2 and -4 in the heart (28). As expected, we also observed in the OE the expression of the CNGA2 subunit of the olfactory CNG channel (data not shown). The identity of mBest2 PCR-amplified fragments was verified by cloning and sequencing. To assess whether splicing or edited variants of mBest2 were expressed in the OE, we cloned the ORF of mBest2 from this tissue by RT-PCR using a DNA polymerase with high proofreading activity. Three independent clones showed 100% identity to BC019528, proving that no OE-specific posttranscriptional modifications occurred.

We examined the cell-type-specific expression of mBest2 by carrying out RT-PCR experiments on a small number of solitary cells from the OE. After enzymatic digestion and mechanical trituration of the adult mouse OE, we harvested single OSNs and supporting cells, purified their RNAs, and performed RT-PCR experiments. By analyzing 2–10 individual OSNs or supporting cells from the OE, we observed that the expression of mBest2 was restricted to OSNs (Fig. 1*b*).

Production of Anti-mBest2 Antibody and Western Blot. To study the expression of the mBest2 protein, we generated a specific polyclonal antibody raised against the C-terminal 144-aa residues of mBest2 (mBest2 344-C-end), a region that is not conserved across bestrophin family members. After transfection of mBest2 cDNA cloned in an expression vector, mBest2 protein was detected in Western blot by the polyclonal antibody as a 57-kDa protein, as expected (Fig. 2*a*). The mBest2-specific band completely disappeared by competition with recombinant GST-mBest2, proving the specificity of the antibody. To assess whether this polyclonal antibody recognizes mBest2 in immunofluorescence experiments, we successfully immunolabeled HEK-293 cells at the cell membrane when transfected with mBest2 cDNA. The staining was abolished when the antibody was preincubated with the recombinant protein (Fig. 2*b*). We tested by Western blot the expression of mBest2 protein in the OE by using a preparation enriched in olfactory cilia. As shown in Fig. 2*c*, mBest2 protein was detected at the expected molecular weight. The signal was completely abolished by preincubation with recombinant GST-mBest2 (data not shown).

Localization of mBest2 on the Cilia of OSNs. The olfactory sensory transduction occurs in specialized cilia extended from the knobs of OSNs on the surface of the OE. To examine the subcellular localization of mBest2 in OSNs, we performed immunohistochemistry experiments on OE cryosection from adult and postnatal day 15 (P15) mice by using the anti-mBest2 polyclonal antibody. We found a homogenous staining on the surface of OE (Fig. 3 *a–c*) without any remarkable difference among the zones of OE in both adult and P15 mice (not shown). The staining was abolished when the antibody was preincubated with the recombinant protein proving signal specificity (data not shown). Specific antibodies against olfactory marker protein (OMP), a typical marker of mature OSNs (34), and the olfactory CNG channel subunit CNGA2 (35), known to be present in the cilia, were used as cellular or subcellular markers. Double staining for mBest2 and OMP showed that mBest2 is expressed in mature OSNs (Fig. 3 *d–f*). Double-staining experiments for mBest2 and CNGA2 proved that mBest2 was present on the luminal surface of the OE (Fig. 3 *e–g*) restricted to the cilia of OSNs, where it colocalized with CNGA2 (higher magnification; Fig. 3 *j–l*). Therefore, mBest2 appears to be expressed at the site of olfactory transduction.

Functional Properties of Ca-Activated Cl Currents from OSNs and mBest2-Transfected HEK-293 Cells. Functional properties of native olfactory Ca-activated Cl currents were measured with the patch–clamp technique from excised inside-out patches from dendritic knob/cilia of mouse OSNs (Figs. 4 , 5, and 7). To compare the functional properties of native olfactory Ca-activated Cl currents with those of heterologously expressed mBest2 currents, we aimed at carrying out a side-by-side comparison in inside-out membrane patches. However, of 78 excised inside-out patches from mBest2- transfected HEK-293 cells, we did not detect any measurable Cl current activated by Ca. A recent report (25) has

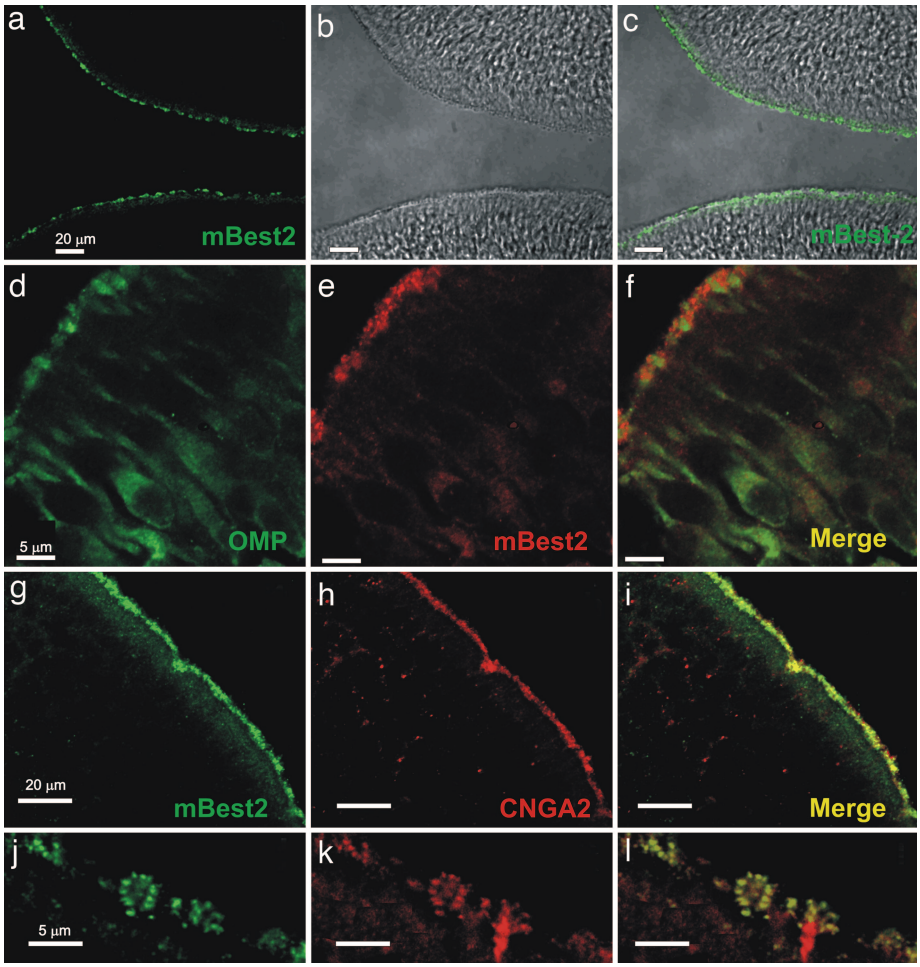

Fig. 3. Localization of mBest2 on the sensory cilia of OSNs. (*a* and *c*) OE (bright field in *b*) labeled with affinity-purified anti-mBest2 polyclonal antibody (green) is shown as the fluorescence signal (*a*) or a digital addition of the fluorescence and bright-field images (*c*). mBest2 is located at the luminal surface of the sensory epithelium. (*d–f*) Double staining for mBest2 (red) and OMP (green). mBest2 was located at the end of dendrites of mature OSNs. (*g–i*) Double staining for mBest2 (green) and CNGA2 (red). Label is shown as the red fluorescence channel digitally combined with the green channel. mBest2 and CNGA2 colocalized at the luminal surface of OE. (*j–l*) Higher magnification of the OE as in *g–i*. mBest2 was expressed on cilia of OSNs and colocalized with CNGA2.

shown that Ca-activated Cl currents induced by heterologous expression of hBest4 could be detected in excised inside-out patches. They suggested, though, that measurements in excised patches could be obtained only because of the particularly large Cl current induced by heterologous expression of hBest4 (24) when compared with the other bestrophins. Here, in the absence of a detectable mBest2-induced current in inside-out patches, we determined the functional properties of mBest2 currents in the whole-cell configuration and those of native Ca-activated Cl currents in the inside-out configuration (Figs. 4–7).

Ca Sensitivity and Single-Channel Conductance. To compare the Ca sensitivity of native olfactory currents with those of mBest2 currents, dose–response relations were obtained by activating currents with various Ca concentrations (Fig. 4). Normalized currents were plotted versus Ca concentration and fitted by the Hill equation. At −50 mV for mBest2 currents, $K_{1/2}$ was 0.4 μM, and n_H was 2.5, whereas for native currents $K_{1/2}$ was 4.7 μM, and n_H was 6.6. mBest2 current amplitudes did not significantly change up to a few minutes of continuous exposure to Ca, whereas the native Ca-activated Cl currents in excised patches displayed a slight inactivation (Fig. 4 *b*, *c*, and *f*). Single-channel events could not be detected even at low Ca concentrations, and therefore we performed stationary noise analysis to estimate the single-channel conductance. By calculating the ratio between variance and mean current at low Ca concentrations, we estimated a single-channel conductance of 0.26 ± 0.06 pS ($n = 4$) for mBest2 and 1.6 ± 0.5 pS ($n = 3$) for native olfactory channels.

Anion Selectivity and Rectification. We replaced NaCl in the bathing solution with NaI, NaBr, $NaNO_3$, or NaMethanesulfonate (NaMeS); measured the shift in reversal potential; and calculated the relative permeability ratios (Fig. 5 *a–c*). Replacement of Cl with MeS shifted the reversal potential from near zero in symmetrical Cl to more positive values for mBest2 (Fig. 5*a*) or to more negative values for native currents (Fig. 5*b*). The measured direction of the shift in reversal potentials was as expected for Cl-selective channels in our experimental conditions, showing that Ca-activated currents were Cl-selective both for mBest2 and for native currents. Fig. 5*c* shows a comparison between the calculated permeability ratios. The same permeability sequence $I > NO_3 > Br > Cl \gg MeS$ was obtained both in native and in mBest2 channels, although the calculated permeability ratios for the various anions were not identical. The current–voltage relations in symmetrical Cl solutions were almost linear (Fig. 5 *a* and *b*), with a slight rectification in opposite directions for native ($I_{+50}/I_{-50} = 0.61 \pm 0.08$) and mBest2 currents ($I_{+50}/I_{-50} = 1.24 \pm 0.04$; Fig. 5*d*).

PHYSIOLOGY

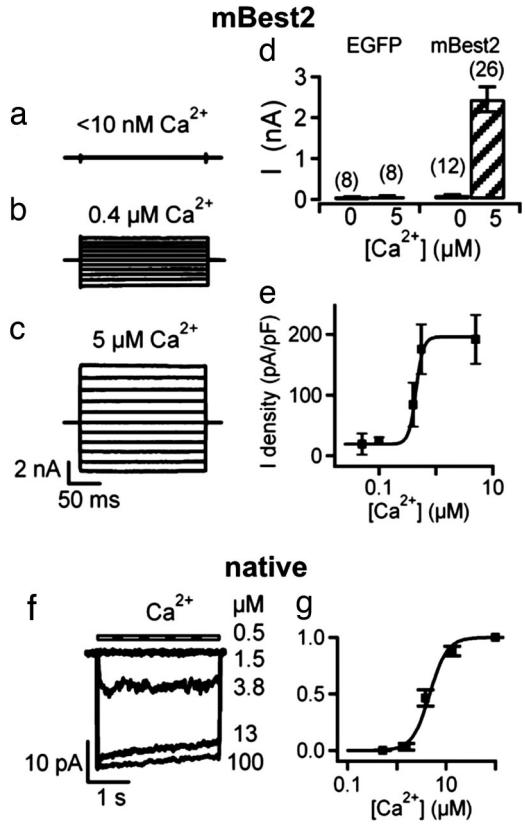

Fig. 4. Calcium sensitivity. (*a*–*e*) mBest2 and EGFP were transfected in HEK-293 cells. Recordings were made 2–3 days after transfection. Whole-cell voltage-clamp recordings were performed with pipette solutions containing <10 nM free Ca (nominally 0 Ca) (*a*), 0.4 μM (*b*), or 5 μM free Ca (*c*). Voltage steps of 200-ms duration were given from a holding potential of 0 mV to voltages between −100 and +100 mV in 20-mV steps. (*d*) Mean steady-state current amplitudes measured at +60 mV in cells transfected with EGFP alone or with mBest2 and EGFP with pipette solutions containing either 0 or 5 μM free Ca. (*e*) Dependence of mBest2 current on intracellular Ca concentration at −50 mV. The amplitude of the average density currents was plotted versus Ca and fitted to the Hill equation with $K_{1/2}$ = 0.4 μM (5–12 cells; solid line). (*f*) A membrane patch was excised from the dendritic knob/cilia of an OSN, and the cytoplasmic side was exposed to the indicated free Ca concentrations at −50 mV. (*g*) Dependence of native current on intracellular Ca concentration fitted to the Hill equation $K_{1/2}$ = 4.7 μM (four patches).

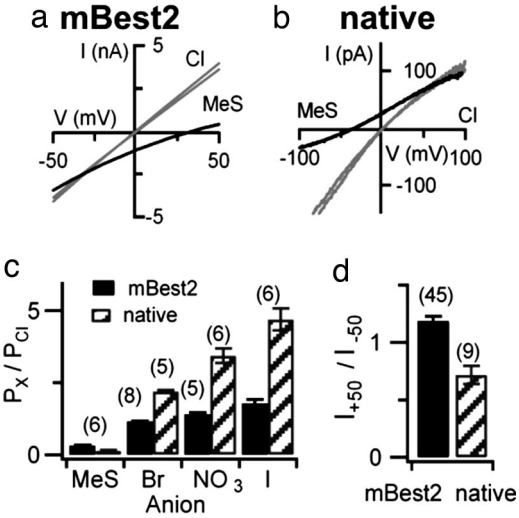

Fig. 5. Anion selectivity. Current-voltage relationships from a ramp protocol measured with bath solutions containing 140 mM NaCl or NaMeS, as indicated for whole-cell mBest2 currents activated by 5 μM Ca (*a*) or native currents activated by 100 μM Ca in an inside-out membrane patch from the dendritic knob/cilia of an OSN (*b*). The two almost-identical traces in symmetrical Cl were measured before and after anion substitution both in *a* and *b*. (*c*) Relative permeability ratios (P_x/P_{Cl}) calculated with the Goldman–Hodgkin–Katz relation from measured reversal potentials were I:NO_3:Br:Cl:MeS = 1.8:1.4:1.2:1:0.3 for mBest2 currents and 4.7:3.4:2.2:1:0.13 for native olfactory currents. (*d*) Rectification of Ca-activated Cl currents calculated as the ratio of currents measured at +50 and −50 mV from experiments as in *a* and *b* in symmetrical Cl.

Extracellular Blockers. Specific blockers for Ca-activated Cl channels with high binding affinity are not available. The most commonly used extracellular blockers of the Ca-activated Cl component of the odorant-induced current in OSNs are 300–500 μM niflumic acid (NFA) and 2–5 mM 4-acetamido-4′-isothiocyanato-stilben-2,2′-disulfonate (SITS; refs. 6, 7, 17, and 36). Here, we investigate the extracellular blockage properties of NFA and SITS on mBest2 currents (Fig. 6). Two millimolar SITS rapidly blocked the Ca-induced current measured at −50 mV and, after SITS removal, the current returned to its initial level (Fig. 6*a*). The blockage by 1 mM NFA was also rapid, and the current slowly recovered toward its original level (Fig. 6*b*). In mBest2-expressing cells, the extracellular application of 1 mM NFA blocked 77 ± 3%, whereas 2 mM SITS blocked 85% ± 4% of the Ca-activated current at −50 mV (Fig. 6*c*). We measured the extracellular SITS blockage in the range from 10 μM to 5 mM and found that it was rapid, reversible, and dose-dependent with a $K_{1/2}$ of 0.4 mM (Fig. 6*d*). The study of the dose dependence of the extracellular blocking effect of NFA in the range from 10 μM to 1 mM revealed a more complex phenomenon. Current blockage by NFA developed with time and reached almost the same steady-state blockage level at every tested concentration, whereas the time necessary to reach steady state was longer as the NFA concentration was decreased (Fig. 6 *e* and *f*). Similar results were obtained at −50 and +50 mV for both NFA and SITS, indicating that their blockage properties on mBest2 current were not voltage-dependent.

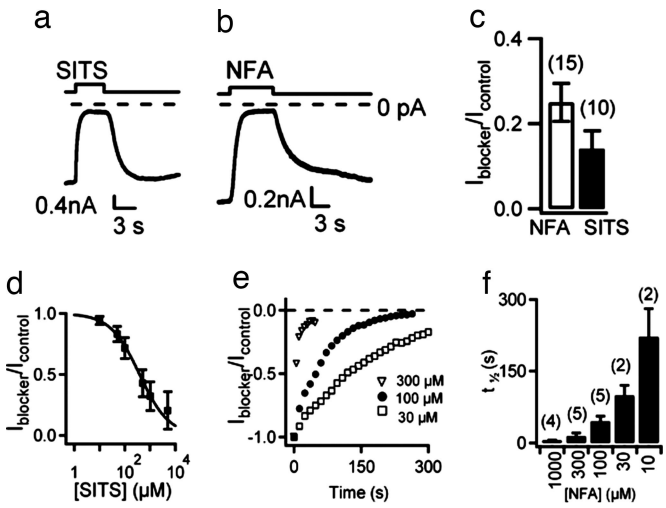

Fig. 6. Extracellular blockage by SITS and NFA on mBest2 currents. HEK-293 cells expressing mBest2 were voltage-clamped at −50 mV with 5 μM intracellular free Ca. Two millimolar SITS (*a*) or 1 mM NFA (*b*) were bath-applied for the time indicated. (*c*) Mean ratios between the amplitudes of the current in the presence and absence of the blocker. (*d*) Sensitivity of mBest2 currents to extracellular SITS. Amplitude of the currents in the presence of various SITS concentrations normalized to control currents was plotted versus SITS concentration and fitted to the Hill equation (five to nine cells). (*e*) Time course of blockage of mBest2 current by various NFA concentrations. (*f*) Time necessary to block half of the current ($t_{1/2}$) at various NFA concentrations.

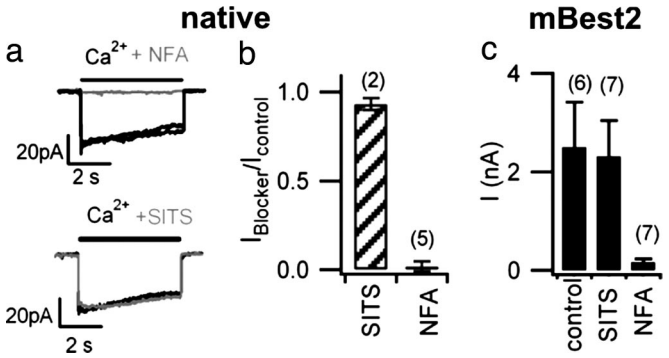

Fig. 7. Intracellular blockage by NFA and SITS. (*a*) Native currents were activated in inside-out patches from dendritic/knob cilia of an OSN by 100 μM Ca at −50 mV. In the same patch, bath application of 1 mM NFA (gray trace, *Upper*) rapidly and reversibly blocked the current, whereas 2 mM SITS (gray trace, *Lower*) did not significantly block the current. Black traces in each image are Ca-activated Cl currents recorded before and after application of each blocker and show the stability of the recordings. (*b*) Ratios between native olfactory Ca-activated Cl currents measured in the presence and absence of SITS or NFA. (*c*) Comparison of average currents measured in mBest2-transfected HEK-293 cells activated by 5 μM intracellular free Ca^{2+} in control and with the intracellular addition of 300 μM NFA or 2 mM SITS.

Intracellular Blockers. We investigated the intracellular blockage properties of NFA and SITS on native olfactory Ca-activated Cl channels in excised inside-out patches. Ca-activated Cl currents were rapidly blocked by the application of 1 mM NFA to the intracellular side (Fig. 7 *a* and *b*), whereas currents were not affected by the addition of 2 mM SITS (Fig. 7 *a* and *b*). The intracellular blockage of NFA or SITS was measured in mBest2 currents by calculating the average whole-cell current activated by 5 μM Ca in the patch pipette in the absence of blockers (control) or in the presence of 300 μM NFA or 2 mM SITS. Intracellular application of 2 mM SITS did not significantly affect Ca-activated mBest2 current, whereas 300 μM NFA blocked most of the current (Fig. 7*c*), similarly to the effects measured on native olfactory Ca-activated Cl currents (Fig. 7*b*).

Discussion

The data presented in this study reveal that mBest2 is expressed in the cilia of OSNs, where it colocalizes with CNGA2, the principal subunit of the CNG olfactory channel responsible for the primary transduction current. Electrophysiological properties of Ca-activated Cl currents of native channels in dendritic/knob cilia of OSNs and of mBest2 expressed in HEK-293 cells are remarkably similar. In fact, both currents have the same anion permeability sequence, small estimated single-channel conductances, current–voltage relations quite close to linearity, and voltage-independent side-specific blockage by NFA and SITS but a Ca sensitivity difference of one order of magnitude. Therefore, the colocalization of mBest2 with CNGA2 on the cilia and the functional data suggest that mBest2 plays a role in olfactory transduction as a molecular component of the ciliary Ca-activated Cl channel. If functional properties of native Ca-activated Cl currents and mBest2 currents are similar, nonetheless they are not identical, and the existing differences indicate the possibility that, as in the case of olfactory CNG channels (reviewed in ref. 33), native channels may be composed of additional proteins.

Comparison of Functional Properties Between Ca-Activated Cl Currents from Knob/Cilia of OSNs and mBest2-Dependent Currents. To functionally compare native Ca-activated Cl currents of OSNs and heterologously expressed mBest2, we performed an electrophysiological analysis of the two currents. A side-by-side comparison in excised inside-out patches for both Ca-dependent currents was not possible, because we did not detect any measurable current in inside-out excised patches from HEK-293 cells expressing mBest2. Therefore, we determined mBest2 functional properties with the whole-cell voltage–clamp technique. Although several properties between native and mBest2 currents were very similar, the nonperfect match could be due to several reasons. First, the use of different recording configurations could produce different results. Second, there could be a lack of posttranslational modification of mBest2 in heterologous systems, such as phosphorylation or sumoylation, that can modulate ion channels (37, 38). Third, ion channels are often composed of more than one type of subunit and/or have additional regulatory proteins that modify the functional properties.

The most significant difference between the two currents was found to be their sensitivity to intracellular Ca. In fact, currents were half-maximal at a Ca concentration of 0.4 μM for mBest2, similar to previous results (19, 21), whereas native currents required a higher Ca concentration, 4.7 μM, in general agreement with micromolar values measured in rat (39) and mouse (17). Dose–response relations obtained from isolated frog olfactory cilia also showed a similar $K_{1/2}$ of 4.8 μM (4). In all cases, there was no significant voltage dependence of Ca activation. Another study (40) measured electrophysiological properties of a Ca-activated Cl current from rat excised patches that did not show similar characteristics to those reported here and by refs. 17 and 39.

The native Ca-activated Cl current slowly inactivated in the presence of a constant Ca concentration when measured in excised patches, as shown by refs. 17 and 39, whereas mBest2 currents in whole-cell recordings did not show any time-dependent change in the presence of any given Ca concentration, as described in refs. 21–23 and 26. However, in isolated frog olfactory cilia, Kleene and Gesteland (4) did not find any current inactivation during prolonged exposure to Ca. The difference in inactivation properties may reflect specific differences between amphibian and mammalian channels or may indicate that some factor remains inside the isolated cilia, whereas it is lost upon excision of the membrane patch.

The current–voltage relations activated by high Ca concentrations in symmetrical Cl solutions were quite close to linearity, with only a moderate inward rectification in native channels, as reported by refs. 4 and 39, and a slight outward rectification in mBest2 currents. Previous reports found a more linear current-voltage relation for mBest2 currents (21, 22).

Single-channel events have not been directly measured because of small unit conductances. The single-channel conductance has been estimated by noise analysis to be 1.6 pS for native channels, in good agreement with previous estimates of 0.5–1.7 pS (39, 41) and 0.3 pS for mBest2 channels. The quite large numerical difference could originate from a different single level of conductance and also from the existence of multiple conductance levels and gating properties in the two channels.

Both native olfactory and mBest2 currents exhibited the same anion permeability sequence $I > NO_3 > Br > Cl \gg MeS$, although the calculated permeability ratios were not identical. This permeability sequence corresponds to the Eisenman "weak field strength" lyotropic series (42), indicating that in both channels, the interaction between the permeant ion and the channel is weak, and permeability is related to the ease with which the permeant ion leaves the bulk solution and enters the channel. Our data are in general agreement with previous measurements (21, 22, 39).

The blocking properties of NFA and SITS were revealed to be similar in native olfactory and mBest2 currents. From the extracellular side, both NFA and SITS block the mBest2 current in the same range of concentration in which the native current is blocked (6, 7, 36). From the intracellular side, only NFA blocks both Ca-activated Cl currents, whereas SITS does not have a

significant effect, in agreement with previous measurements in frog olfactory cilia (5, 15).

Mechanism of Ca Activation. Native olfactory channels appear to be rapidly activated by Ca in inside-out patches (see also refs. 17 and 39) and in isolated olfactory cilia (4, 5), whereas similar experiments for Ca activation of mBest2 are missing. A recent study (25) has shown that hBest4 can be activated by Ca in excised inside-out patches, indicating that diffusible messengers or protein phosphorylation are not implicated in Ca activation. However, because the current activates and deactivates very slowly in response to Ca (time constant of 10–20 seconds), indirect Ca activation through a membrane-associated messenger cannot be excluded. Tsunenari *et al.* (25) also suggest that, alternatively, Ca could directly bind to hBest4, but that the binding controls the channel through another entity. Because bestrophin homologues have different channel kinetics and voltage dependencies (23, 24), we cannot exclude that each bestrophin has a different gating mechanism, as in the case of the TRP family of ion channels (43). We have found that mBest2 is the only bestrophin expressed in the OE. Site-directed mutagenesis experiments have demonstrated (21, 22, 26) that the putative second transmembrane domain of mBest2 participates in forming the channel pore, and therefore mBest2 appears to be at least part of the pore. However, it might also be possible that mBest2 forms a heteromultimer with other channel subunits, or that it has associated proteins that may, for example, modify Ca sensitivity and inactivation properties. It is likely that future studies will identify additional molecular components and/or modulators of the native olfactory Ca-activated Cl channel.

Conclusions

The colocalization of mBest2 with CNGA2 on the cilia of OSNs, together with the functional data, strongly indicates that mBest2 mediates the Ca-activated Cl current involved in olfactory transduction. Future studies should examine the involvement of additional components in forming and/or modulating the native olfactory channel. Our results contribute to the elucidation of the molecular mechanisms underlying olfactory transduction and provide further information about the physiological role of bestrophins. Indeed, our data indicate that olfactory transduction is a good experimental system to study the physiological function of mBest2.

Materials and Methods

RT-PCR and Single-Cell RT-PCR. Tissue and single neurons were obtained from adult C57Black/6 mice. A description of the method is given in *Supporting Text*, which is published as supporting information on the PNAS web site.

Production of an Anti-mBest2 Polyclonal Antibody. Antibody was raised by immunization of rabbit using GST-C-terminal 431-bp mBest2 fusion protein (for details, see *Supporting Text*).

Cell Culture, Transfections, and Immunoblot. HEK-293 cells were transfected with mBest2 construct in pCMV-Sport6 by using FuGENE 6 reagent (Roche Diagnostics, Indianapolis, IN). For Western blot, membrane fractions enriched in olfactory cilia from OSNs were obtained with the calcium-shock method according to ref. 44 (see *Supporting Text*).

Immunofluorescence. Immunolabeling was performed by standard protocols for tissue fixation and processing (see *Supporting Text*). The staining was analyzed by confocal microscopy.

Electrophysiology. mBest2 currents were recorded in the whole-cell patch–clamp configuration from HEK-293 transfected cells. Native olfactory currents were recorded in inside-out patches excised from the dendritic knob/cilia of OSNs, obtained by enzymatic dissociation of the OE of 4- to 8-week-old C57Black/6 and BALB/c mice, as described (45, 46). For details, see *Supporting Text*. Averaged values are mean ± SEM. In the figures, the number of recorded cells or patches is indicated in parentheses; error bars indicate SEM.

We thank L. Buck, M. Pusch, R. Tirindelli, P. Pelosi, E. Cherubini, A. Nistri, and V. Torre for interesting discussions; F. Margolis (University of Maryland, Baltimore, MD) for the gift of the OMP antibody; F. Müller and U. B. Kaupp (Forschungszentrum Julich, Julich, Germany) for the gift of the CNGA2 monoclonal antibody; M. Stebel for mBest2 polyclonal antibody production; L. Masten for OE and ciliary membrane preparations; C. Patton for discussion on Ca buffering; B. Cataletto, M. Celussi, and G. Adami for help with calcium measurements; L. De Maso for technical help; and M. Schipizza-Lough for checking the English. This work was supported by European Union Grant NFG 503221, the Giovanni Armenise–Harvard Foundation, and the Istituto Italiano di Tecnologia.

1. Schild, D. & Restrepo, D. (1998) *Physiol. Rev.* **78,** 429–466.
2. Buck, L. B. (2000) *Cell* **100,** 611–618.
3. Menini, A., Lagostena, L. & Boccaccio, A. (2004) *News Physiol. Sci.* **19,** 101–104.
4. Kleene, S. J. & Gesteland, R. C. (1991) *J. Neurosci.* **11,** 3624–3629.
5. Kleene, S. J. (1993) *Neuron* **11,** 123–132.
6. Lowe, G. & Gold, G. H. (1993) *Nature* **366,** 283–286.
7. Kurahashi, T. & Yau, K. W. (1993) *Nature* **363,** 71–74.
8. Kaneko, H., Nakamura, T. & Lindemann, B. (2001) *Am. J. Physiol.* **280,** C1387–C1393.
9. Reuter, D., Zierold, K., Schroder, W. H. & Frings, S. (1998) *J. Neurosci.* **18,** 6623–6630.
10. Nakamura, T., Kaneko, H. & Nishida, N. (1997) *Neurosci. Lett.* **237,** 5–8.
11. Zhainazarov, A. B. & Ache, B. W. (1995) *J. Neurophysiol.* **74,** 479–483.
12. Kleene, S. J. (1997) *Biophys. J.* **73,** 1110–1117.
13. Matthews, H. R. & Reisert, J. (2003) *Curr. Opin. Neurobiol.* **13,** 469–475.
14. Menini, A. (1999) *Curr. Opin. Neurobiol.* **9,** 419–426.
15. Frings, S., Reuter, D. & Kleene, S. J. (2000) *Prog. Neurobiol.* **60,** 247–289.
16. Kaneko, H., Putzier, I., Frings, S., Kaupp, U. B. & Gensch, T. (2004) *J. Neurosci.* **24,** 7931–7938.
17. Reisert, J., Lai, J., Yau, K. W. & Bradley, J. (2005) *Neuron* **45,** 553–561.
18. Nickell, W. T., Kleene, N. K., Gesteland, R. C. & Kleene, S. J. (2006) *J. Neurophysiol.* **95,** 2003–2006.
19. Qu, Z., Wei, R. W., Mann, W. & Hartzell, H. C. (2003) *J. Biol. Chem.* **278,** 49563–49572.
20. Hartzell, C., Qu, Z., Putzier, I., Artinian, L., Chien, L. T. & Cui, Y. (2005) *Physiology (Bethesda)* **20,** 292–302.
21. Qu, Z., Fischmeister, R. & Hartzell, C. (2004) *J. Gen. Physiol.* **123,** 327–340.
22. Qu, Z. & Hartzell, C. (2004) *J. Gen. Physiol.* **124,** 371–382.
23. Sun, H., Tsunenari, T., Yau, K. W. & Nathans, J. (2002) *Proc. Natl. Acad. Sci. USA* **99,** 4008–4013.
24. Tsunenari, T., Sun, H., Williams, J., Cahill, H., Smallwood, P., Yau, K. W. & Nathans, J. (2003) *J. Biol. Chem.* **278,** 41114–41125.
25. Tsunenari, T., Nathans, J. & Yau, K. W. (2006) *J. Gen. Physiol.* **127,** 749–754.
26. Qu, Z., Chien, L. T., Cui, Y. & Hartzell, H. C. (2006) *J. Neurosci.* **26,** 5411–5419.
27. Hartzell, C., Putzier, I. & Arreola, J. (2005) *Annu. Rev. Physiol* **67,** 719–758.
28. Kramer, F., Stohr, H. & Weber, B. H. (2004) *Cytogenet. Genome Res.* **105,** 107–114.
29. Petrukhin, K., Koisti, M. J., Bakall, B., Li, W., Xie, G., Marknell, T., Sandgren, O., Forsman, K., Holmgren, G., Andreasson, S., *et al.* (1998) *Nat. Genet.* **19,** 241–247.
30. Marquardt, A., Stohr, H., Passmore, L. A., Kramer, F., Rivera, A. & Weber, B. H. (1998) *Hum. Mol. Genet.* **7,** 1517–1525.
31. White, K., Marquardt, A. & Weber, B. H. (2000) *Hum. Mutat.* **15,** 301–308.
32. Pusch, M. (2004) *J. Gen. Physiol.* **123,** 323–325.
33. Kaupp, U. B. & Seifert, R. (2002) *Physiol. Rev.* **82,** 769–824.
34. Keller, A. & Margolis, F. L. (1975) *J. Neurochem.* **24,** 1101–1106.
35. Meyer, M. R., Angele, A., Kremmer, E., Kaupp, U. B. & Muller, F. (2000) *Proc. Natl. Acad. Sci. USA* **97,** 10595–10600.
36. Kurahashi, T. & Menini, A. (1997) *Nature* **385,** 725–729.
37. Muller, F., Vantler, M., Weitz, D., Eismann, E., Zoche, M., Koch, K. W. & Kaupp, U. B. (2001) *J. Physiol.* **532,** 399–409.
38. Rajan, S., Plant, L. D., Rabin, M. L., Butler, M. H. & Goldstein, S. A. (2005) *Cell* **121,** 37–47.
39. Reisert, J., Bauer, P. J., Yau, K. W. & Frings, S. (2003) *J. Gen. Physiol.* **122,** 349–363.
40. Hallani, M., Lynch, J. W. & Barry, P. H. (1998) *J. Membr. Biol.* **161,** 163–171.
41. Larsson, H. P., Kleene, S. J. & Lecar, H. (1997) *Biophys. J.* **72,** 1193–1203.
42. Eisenman, G. & Horn, R. (1983) *J. Membr. Biol.* **76,** 197–225.
43. Clapham, D. E. (2003) *Nature* **426,** 517–524.
44. Pace, U., Hanski, E., Salomon, Y. & Lancet, D. (1985) *Nature* **316,** 255–258.
45. Lagostena, L. & Menini, A. (2003) *Chem. Senses* **28,** 705–716.
46. Boccaccio, A., Lagostena, L., Hagen, V. & Menini, A. (2006) *J. Gen. Physiol.* **128,** 171–184.